

Quenching the Anisotropic Heisenberg Chain: Exact Solution and Generalized Gibbs Ensemble

B. Wouters,¹ M. Brockmann,¹ J. De Nardis,¹ D. Fioretto,¹ M. Rigol,² and J.-S. Caux¹

¹*Institute for Theoretical Physics, University of Amsterdam, Science Park 904
Postbus 94485, 1090 GL Amsterdam, The Netherlands*

²*Department of Physics, The Pennsylvania State University, University Park, Pennsylvania 16802, USA*
(Dated: September 1, 2022)

We study quenches in integrable spin-1/2 chains in which we evolve the ground state of the antiferromagnetic Ising model with the anisotropic Heisenberg Hamiltonian. For this nontrivially interacting situation, an application of the first-principles-based quench action method allows us to give an exact description of the post-quench steady state in the thermodynamic limit. We show that a generalized Gibbs ensemble, implemented using all known local conserved charges, fails to reproduce the exact quench action steady state and to correctly predict post-quench equilibrium expectation values of physical observables. This is supported by numerical linked-cluster calculations within the diagonal ensemble in the thermodynamic limit.

PACS numbers: 02.30.Ik, 05.70.Ln, 75.10.Jm

Introduction. Out-of-equilibrium phenomena are of importance throughout physics, in fields ranging from cosmology [1] and superfluid helium [2], heavy-ion collisions [3], pattern formation [4], exclusion processes [5], glasses [6] all the way to atomic-scale isolated quantum systems [7]. Much recent experimental and theoretical activity has been focused on the latter, raising fundamental questions as to whether, how and to what state such systems relax under unitary time evolution following a sudden quantum quench [8–42]. From this work, two scenarios for equilibration have emerged, one applicable to models having only a few local conserved quantities, the other relevant to integrable models characterized by an infinite number of local conserved charges. In the former, thermalization to a Gibbs ensemble is the rule [11], while in the latter, equilibration to a so-called Generalized Gibbs Ensemble (GGE) [9, 10] is generally thought to occur, in particular for lattice spin systems [12–20].

In this letter, we study a quench in which the second scenario breaks down. Our initial state, defined as a purely antiferromagnetic (spin-1/2 Néel) state, is let to evolve unitarily in time according to the XXZ spin chain Hamiltonian. This is a physically meaningful quench protocol, which can in principle be implemented using for example cold atoms [43–47]. We provide a thermodynamically exact solution for the steady state reached long after the quench, derived directly from microscopics using the recently-proposed quench action method [48]. The solution takes the form of a set of distributions of quasi-momenta that completely characterizes the macrostate representing the steady state, from which observables of interest can be calculated. As a stringent test, it correctly reproduces the expectation values of all local conserved charges. Furthermore, we implement a numerical linked-cluster expansion (NLCE) [49, 50] whose results support the correctness of the quench action approach. Our application of the latter to nontrivially interacting lattice

models follows up on the recent quench action solution of interaction quenches in one-dimensional Bose systems [51], and demonstrates the broad applicability of the approach.

Besides providing the exact solution using the quench action, we explicitly construct a GGE for the Néel-to-XXZ quench using all known local conserved charges, enabling an analytical check of the GGE logic applied to interacting systems. We show that it fails to reproduce the steady state as predicted by the quench action. As a consequence, equilibrium expectation values of physical observables are predicted differently by the quench action method, which corresponds to the prediction of the diagonal ensemble, and the GGE based on all known local conserved charges. We display these differences explicitly for short-distance spin-spin correlations and verify them using NLCE. Our results highlight how far-from-equilibrium dynamics can reveal the effects of physically relevant but unknown conserved quantities in interacting integrable models.

Quench protocol. Our initial state is the ground state of the antiferromagnetic Ising model, namely, the translationally invariant Néel state

$$|\Psi_0\rangle = \frac{1}{\sqrt{2}} (|\uparrow\downarrow\uparrow\downarrow\dots\rangle + |\downarrow\uparrow\downarrow\uparrow\dots\rangle). \quad (1)$$

The time evolution after the quench is governed by the antiferromagnetic XXZ spin chain Hamiltonian

$$H = \frac{J}{4} \sum_{j=1}^N [\sigma_j^x \sigma_{j+1}^x + \sigma_j^y \sigma_{j+1}^y + \Delta(\sigma_j^z \sigma_{j+1}^z - 1)], \quad (2)$$

with exchange coupling $J > 0$. The Néel state is the ground-state in the limit $\Delta \rightarrow \infty$. The Pauli matrices σ_j^α ($\alpha = x, y, z$) represent the spin-1/2 degrees of freedom at lattice sites $j = 1, 2, \dots, N$, and we assume periodic boundary conditions $\sigma_{N+1}^\alpha = \sigma_1^\alpha$. We restrict our

analysis to quenches for which $\Delta \geq 1$ (details for the $\Delta = 1$ case are provided in Ref. [52]).

Eigenstates of the Hamiltonian (2) can be obtained by Bethe Ansatz [53]. Each normalized Bethe wavefunction

$$|\boldsymbol{\lambda}\rangle = \sum_{\mathbf{x}} \sum_Q A_Q(\boldsymbol{\lambda}) \prod_{j=1}^M e^{ix_j p(\lambda_{Q_j})} \sigma_{x_j}^- |\uparrow \uparrow \dots \uparrow\rangle \quad (3)$$

lies in a fixed magnetization sector $\langle \sigma_{\text{tot}}^z \rangle / 2 = N/2 - M$. It is completely specified by a set of complex quasi-momenta, or rapidities, $\boldsymbol{\lambda} = \{\lambda_k\}_{k=1}^M$, which satisfy the Bethe equations

$$\left(\frac{\sin(\lambda_j + i\eta/2)}{\sin(\lambda_j - i\eta/2)} \right)^N = - \prod_{k=1}^M \frac{\sin(\lambda_j - \lambda_k + i\eta)}{\sin(\lambda_j - \lambda_k - i\eta)}, \quad (4)$$

for $j = 1, \dots, M$. The parameter $\eta > 0$ is related to the anisotropy parameter $\Delta = \cosh(\eta)$. The first sum in Eq. (3) is over all ordered configurations $\mathbf{x} = \{x_j\}_{j=1}^M \subset \{1, \dots, N\}$ of down spin positions, while the second sum runs over all permutations Q of labels $\{1, \dots, M\}$. $A_Q(\boldsymbol{\lambda})$ are rapidity-dependent amplitudes [53]. The total momentum and energy of a Bethe state are given by

$$P_{\boldsymbol{\lambda}} = \sum_{j=1}^M p(\lambda_j), \quad p(\lambda) = i \ln \left[\frac{\sin(\lambda - i\eta/2)}{\sin(\lambda + i\eta/2)} \right], \quad (5)$$

$$\omega_{\boldsymbol{\lambda}} = \sum_{j=1}^M e(\lambda_j), \quad e(\lambda) = -J\pi \sinh(\eta) a_1(\lambda), \quad (6)$$

where $a_1(\lambda) = \sinh(\eta) / [\pi(\cosh \eta - \cos 2\lambda)]$.

Bethe states are classified according to the string hypothesis [54, 55]. Rapidities arrange themselves in strings $\lambda_{\alpha}^{n,a} = \lambda_{\alpha}^n + \frac{i\eta}{2}(n+1-2a) + i\delta_{\alpha}^{n,a}$, $a = 1, \dots, n$, where n is the length of the string and the deviations $\delta_{\alpha}^{n,a}$ vanish (typically exponentially) upon taking the infinite-size limit. For $\Delta > 1$ the string centers λ_{α}^n lie in the interval $[-\pi/2, \pi/2)$. Physically, such an n -string corresponds to a bound state of n magnons, which in the Ising limit $\Delta \rightarrow \infty$ can be seen as a block of n adjacent down spins.

At time t after the quench, the state of the system can be expanded in the basis of Bethe states such that the post-quench time-dependent expectation value of a generic operator \mathcal{O} is exactly given by the double sum

$$\langle \Psi(t) | \mathcal{O} | \Psi(t) \rangle = \sum_{\boldsymbol{\lambda}, \boldsymbol{\lambda}'} e^{-S_{\boldsymbol{\lambda}}^* - S_{\boldsymbol{\lambda}'}} e^{i(\omega_{\boldsymbol{\lambda}} - \omega_{\boldsymbol{\lambda}'})t} \langle \boldsymbol{\lambda} | \mathcal{O} | \boldsymbol{\lambda}' \rangle, \quad (7)$$

with overlap coefficients $S_{\boldsymbol{\lambda}} = -\ln \langle \boldsymbol{\lambda} | \Psi_0 \rangle$.

Quench action. The double sum over the full Hilbert space in Eq. (7) represents a substantial bottleneck, its size growing exponentially with N . The quench action method [48, 51] gives a handle on this double sum in the thermodynamic limit $N \rightarrow \infty$ (with $M/N = 1/2$ fixed), denoted by \lim_{th} . In this limit, a state is characterized by the distributions of its string centers. They are given

by a set of positive, smooth and bounded densities $\boldsymbol{\rho} = \{\rho_n\}_{n=1}^{\infty}$ for the string centers λ_{α}^n , representing a set of Bethe states with Yang-Yang entropy

$$\frac{S_{YY}[\boldsymbol{\rho}]}{N} = \sum_{n=1}^{\infty} \int_{-\pi/2}^{\pi/2} d\lambda [\rho_n \ln(1 + \eta_n) + \rho_{n,h} \ln(1 + \eta_n^{-1})]. \quad (8)$$

Here, $\rho_{n,h}$ is the density of holes of n -string centers [56, 57], $\eta_n = \rho_{n,h}/\rho_n$, and we leave the λ -dependence implicit. The Bethe Eqs. (4) become a set of coupled integral equations [55] for the densities $\boldsymbol{\rho}$:

$$\rho_n(1 + \eta_n) = s * (\eta_{n-1}\rho_{n-1} + \eta_{n+1}\rho_{n+1}), \quad n \geq 1, \quad (9)$$

with $\eta_0(\lambda) = 1$ and $\rho_0(\lambda) = \delta(\lambda)$. The convolution $*$ is defined by $(f * g)(\lambda) = \int_{-\pi/2}^{\pi/2} f(\lambda - \mu)g(\mu)d\mu$, and the kernel in Eq. (9) is $s(\lambda) = \frac{1}{2\pi} \sum_{k \in \mathbb{Z}} \frac{e^{-2ik\lambda}}{\cosh(k\eta)}$.

As explained in Ref. [51], for a large class of physical observables, the double sum in Eq. (7) can be recast in the thermodynamic limit as a functional integral over the root densities $\boldsymbol{\rho}$. The weight of the functional integral $e^{-S_{QA}[\boldsymbol{\rho}]}$ is given by the quench action $S_{QA}[\boldsymbol{\rho}] = 2S[\boldsymbol{\rho}] - S_{YY}[\boldsymbol{\rho}]$, where $S[\boldsymbol{\rho}] = \lim_{\text{th}} \text{Re } S_{\boldsymbol{\lambda}}$ is the extensive real part of the overlap coefficient in the thermodynamic limit. Since the quench action is extensive, real and bounded from below, a saddle-point approximation becomes exact in the thermodynamic limit. At long times after the quench, the system relaxes to a steady state $\boldsymbol{\rho}^{\text{SP}}$ determined by the variational equations

$$0 = \left. \frac{\delta S_{QA}[\boldsymbol{\rho}]}{\delta \rho_n(\lambda)} \right|_{\boldsymbol{\rho}=\boldsymbol{\rho}^{\text{SP}}} \quad \text{for } n \geq 1. \quad (10)$$

Steady-state expectation values of physical observables can then be effectively computed on this state:

$$\lim_{t \rightarrow \infty} \lim_{\text{th}} \langle \Psi(t) | \mathcal{O} | \Psi(t) \rangle = \langle \boldsymbol{\rho}^{\text{SP}} | \mathcal{O} | \boldsymbol{\rho}^{\text{SP}} \rangle. \quad (11)$$

The saddle-point distributions of string centers $\boldsymbol{\rho}^{\text{SP}}$ thus encode all equilibrium expectation values and correlators of physical observables after the quench [14, 48].

The implementation of the quench action approach to the Néel-to-XXZ quench proceeds as follows (see Ref. [58] for details). One of the main ingredients is the leading order behavior of the overlaps $\langle \boldsymbol{\lambda} | \Psi_0 \rangle$ in the thermodynamic limit. It was proven in Refs. [59, 60] (starting from Ref. [61]) that only overlaps between $|\Psi_0\rangle$ and parity-invariant Bethe states are nonvanishing; practical determinant expressions were also derived. Taking M to be even, rapidities of parity-invariant states come in pairs such that $\{\lambda_j\}_{j=1}^M = \{-\lambda_j\}_{j=1}^M$ and the overlap is now determined by $M/2$ rapidities $\tilde{\boldsymbol{\lambda}} = \{\lambda_j\}_{j=1}^{M/2}$. The overlap's leading term (in system size) reads [59]

$$\langle \tilde{\boldsymbol{\lambda}} | \Psi_0 \rangle \sim \prod_{j=1}^{M/2} \frac{\sqrt{\tan(\lambda_j + i\eta/2) \tan(\lambda_j - i\eta/2)}}{2 \sin(2\lambda_j)}. \quad (12)$$

One can straightforwardly separate the contributions of different string lengths and derive an expression for the thermodynamic overlap coefficients $S[\rho]$. Before varying the quench action, as per Eq. (10), one needs to add a Lagrange multiplier fixing the filling of the saddle-point state to the Néel state's $\lim_{\text{th}} M/N = 1/2$. Variation leads to a set of Generalized Thermodynamic Bethe Ansatz (GTBA) equations for the functions η_n [58],

$$\ln(\eta_n) = d_n + s * [\ln(1 + \eta_{n-1}) + \ln(1 + \eta_{n+1})], \quad (13)$$

where $n \geq 1$, $\eta_0(\lambda) = 0$ by convention, and

$$d_n(\lambda) = \sum_{k \in \mathbb{Z}} e^{-2ik\lambda} \frac{\tanh(\eta k)}{k} [(-1)^n - (-1)^k]. \quad (14)$$

The solution to the GTBA Eqs. (13), substituted into the Bethe Eqs. (9), leads to a set of root densities ρ^{SP} describing the steady state of the Néel-to-XXZ quench. They can be numerically computed by truncating the infinite sets of Eqs. (13) and (9). In Figs. 1(a) and 1(b), we plot saddle-point distributions of 1- and 2-strings for different values of Δ . A notable feature is the vanishing of the even-length string densities at $\lambda = 0$, which corresponds to the fact that the overlaps (12) between the Néel state and parity-invariant Bethe states with a string of even length centered at zero identically vanish. Furthermore, for large Δ the density of 1-strings becomes increasingly dominant, approaching the ground state of the Ising model [$\rho_1(\lambda) = 1/(2\pi)$ and $\rho_n(\lambda) = 0$ for $n \geq 2$], in accordance with the expected result for the quenchless point $\Delta = \infty$.

NLCE. Our NLCE follows on Ref. [49] and has been tailored to solve the specific quench studied in this work [50, 58]. NLCEs enable the calculation of the infinite-time average (also known as the diagonal ensemble result) of correlation functions after the quench in the thermodynamic limit [49, 50]. The idea is that any spin-spin correlation can be computed as a sum over the contributions from all connected clusters c that can be embedded on the lattice, $\langle \sigma_i^z \sigma_j^z \rangle_{\text{NLCE}} = \sum_c M(c) \times \mathcal{W}_{\sigma_i^z \sigma_j^z}(c)$, where $M(c)$ is the number of embeddings of c per site, and $\mathcal{W}_{\sigma_i^z \sigma_j^z}(c)$ is the weight of $\sigma_i^z \sigma_j^z$ in c . The latter is calculated using the inclusion-exclusion principle, $\mathcal{W}_{\sigma_i^z \sigma_j^z}(c) = \langle \sigma_i^z \sigma_j^z \rangle_c^{\text{DE}} - \sum_{s \subset c} \mathcal{W}_{\sigma_i^z \sigma_j^z}(s)$, where the last sum runs over all connected sub-clusters of c , and $\langle \sigma_i^z \sigma_j^z \rangle_c^{\text{DE}} = \text{Tr}[\sigma_i^z \sigma_j^z \hat{\rho}_c^{\text{DE}}] / \text{Tr}[\hat{\rho}_c^{\text{DE}}]$ is the expectation value of $\sigma_i^z \sigma_j^z$ calculated with the density matrix in the diagonal ensemble $\hat{\rho}_c^{\text{DE}}$ (in cluster c). In order to accelerate the convergence of the NLCE, we use Wynn's and Brezinski's resummation algorithms [58, 62, 63].

GGE. The integrable structure of the XXZ spin chain provides, in the thermodynamic limit, an infinite set of local conserved charges Q_m , $m \in \mathbb{N}$, such that $Q_1 \propto P$, $Q_2 \propto H$ [64, 65]. For integrable models, it is conjectured (and shown for specific quenches) that the steady

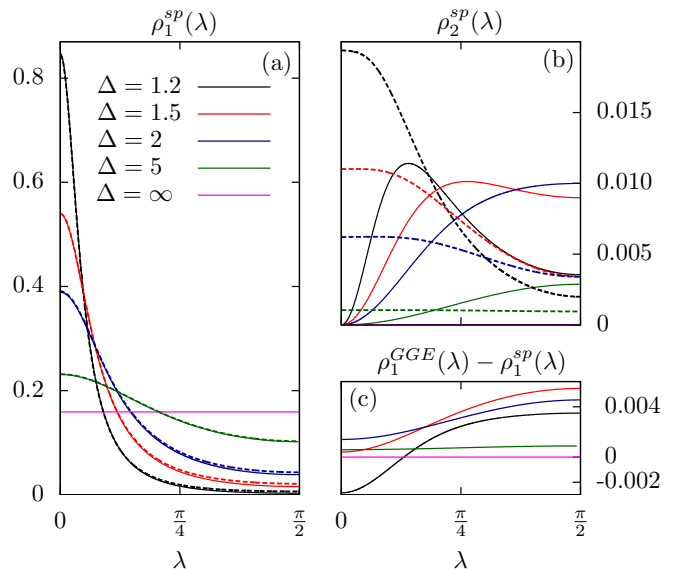


FIG. 1. (color online) (a) and (b): Density functions ρ_1 and ρ_2 for the quench to different values of $\Delta > 1$ of both the quench action saddle-point state (solid lines) and the GGE equilibrium state (dashed lines). (c): Difference between the GGE prediction for ρ_1 and the quench action saddle-point result. All distributions are symmetric functions of $\lambda \in [-\pi/2, \pi/2]$.

state after a quench can be described by a GGE. For the XXZ spin chain, the latter is given by a set of densities ρ^{GGE} which maximizes the Yang-Yang entropy $S_{YY}[\rho]$ under the constraint of fixed expectation values of the local conserved charges Q_m [66, 67]. This translates into GTBA equations of the same form as Eqs. (13), but now with the driving function d_1 determined by the chemical potentials associated with the charges, and the remaining $d_n(\lambda) = 0$ for $n \geq 2$. Together with Eqs. (9), this uniquely determines ρ^{GGE} . In general, the values of the chemical potentials are inaccessible for the XXZ model, except for a truncated GGE when only a small number of conserved charges is taken into account [36].

However, it turns out that the expectation values of all local conserved charges Q_m on the initial state are in one-to-one correspondence with the density $\rho_{1,h}$ of 1-string holes, i.e.,

$$\lim_{\text{th}} \left(\frac{\langle \Psi_0 | Q_{2m+2} | \Psi_0 \rangle}{N \sinh^{2m+1}(\eta)} \right) = \sum_{k \in \mathbb{Z}} \frac{\hat{\rho}_{1,h}(k) - e^{-|k|\eta}}{2 \cosh(k\eta)} (ik)^{2m}, \quad (15)$$

with $m \geq 0$ and $\hat{\rho}_{1,h}$ the Fourier transform of $\rho_{1,h}$, see Ref. [58]. In the case of the Néel-to-XXZ quench, the expectation values of the conserved charges on the initial state [68] fix $\rho_{1,h}$ unambiguously [52]:

$$\rho_{1,h}^{\text{Néel}}(\lambda) = \frac{\pi^2 a_1^3(\lambda) \sin^2(2\lambda)}{\pi^2 a_1^2(\lambda) \sin^2(2\lambda) + \cosh^2(\eta)}, \quad (16)$$

where a_1 was defined right after Eq. (6). This makes

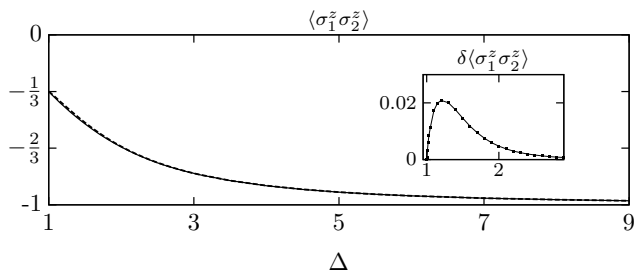


FIG. 2. (color online) Correlator $\langle \sigma_1^z \sigma_2^z \rangle$ evaluated on the quench action steady state (solid lines) and on the GGE (dashed lines). The energy sum rule $2\langle \sigma_1^x \sigma_2^x \rangle + \Delta \langle \sigma_1^z \sigma_2^z \rangle = -\Delta$ explains the exact value of $-1/3$ at the isotropic point $\Delta = 1$. Numerical errors are 10^{-5} or smaller. Both sets of data are in agreement with the finite-size computations of Ref. [19], within the numerical precision of the latter. *Inset*: Relative difference between the GGE prediction and the quench action saddle-point result, $\delta \langle \sigma_1^z \sigma_2^z \rangle = 1 - \langle \sigma_1^z \sigma_2^z \rangle_{\text{GGE}} / \langle \sigma_1^z \sigma_2^z \rangle_{\text{sp}}$.

the input from the chemical potentials redundant. The densities ρ^{GGE} for the GGE can be found by solving the GTBA Eqs. (13) for $n \geq 2$ [$d_n(\lambda) = 0$] and the Bethe Eqs. (9) with the constraint $\rho_{1,h}^{\text{GGE}} = \rho_{1,h}^{\text{Néel}}$.

Discussion of results. Numerical and analytical analysis show exact agreement between $\rho_{1,h}$ predicted by the quench action approach and $\rho_{1,h}^{\text{Néel}}$ in Eq. (16) [52]. The expectation values of all local conserved charges Q_n are thus reproduced exactly. We stress that this nontrivial agreement constitutes strong evidence for the correctness of the quench action prediction of the steady state.

Furthermore, the distributions of the GGE can be compared with the steady state distributions provided by the quench action approach, see Fig. 1. The densities ρ_n for the GGE and the quench action are clearly different, the discrepancies becoming more pronounced as one reduces the anisotropy towards the gapless point $\Delta = 1$. We emphasize that all our results are obtained in the thermodynamic limit: these differences are not finite size effects.

We verified the existence of these discrepancies by analytically solving the GTBA equations of the two ensembles in a large- Δ expansion. The differences between the distributions are of order Δ^{-2} , e.g., for 1- and 2-strings (for other strings and higher orders, see Ref. [52])

$$\rho_1^{\text{GGE}}(\lambda) - \rho_1^{\text{sp}}(\lambda) = \frac{1}{4\pi\Delta^2} + O(\Delta^{-3}), \quad (17a)$$

$$\rho_2^{\text{GGE}}(\lambda) - \rho_2^{\text{sp}}(\lambda) = \frac{1 - 3\sin^2(\lambda)}{3\pi\Delta^2} + O(\Delta^{-3}). \quad (17b)$$

Given steady state distributions, one can compute physical observables [Eq. (11)]. Nonvanishing differences between distributions will generally be reflected in those expectation values, even in simple ones such as few-point spin-spin correlation functions. We have implemented an adapted version of the Hellmann-Feynman theorem

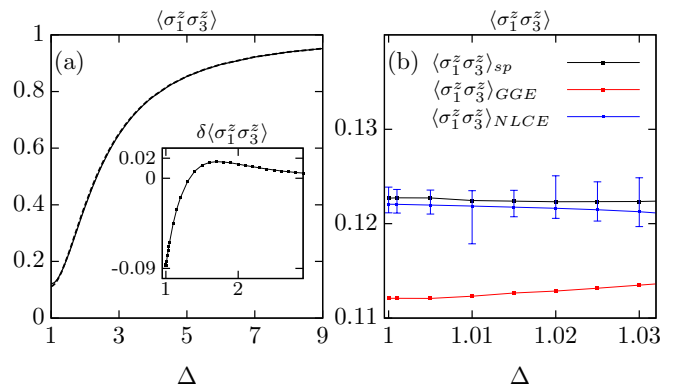


FIG. 3. (color online) (a) The same as Fig. 2 for $\langle \sigma_1^z \sigma_3^z \rangle$. (b) Comparison between the quench action, the GGE prediction, and the NLCE result close to the isotropic point. Error-bars in the NLCE data display an interval of confidence that includes all resummation results (except for $\Delta = 1.015$) [58].

to compute the expectation value $\langle \sigma_1^z \sigma_2^z \rangle$ from the distributions ρ [58, 69]. The nearest-neighbor two-point correlator is predicted differently by the quench action steady state and the GGE (see Fig. 2). The NLCE results (not shown) are consistent with those predictions but cannot resolve their difference since it is too small ($\lesssim 2\%$, as shown in the inset in Fig. 2). It should be noted that the magnitude of differences between distributions in Eqs. (17) does not directly translate into a similar difference for physical observables. Expanding for large anisotropy, we obtain a discrepancy of order Δ^{-6} :

$$\langle \sigma_1^z \sigma_2^z \rangle_{\text{GGE}} - \langle \sigma_1^z \sigma_2^z \rangle_{\text{sp}} = \frac{9}{16\Delta^6} + O(\Delta^{-7}). \quad (18)$$

We also calculate the next-nearest-neighbor correlator $\langle \sigma_1^z \sigma_3^z \rangle$ by means of the method of Ref. [69], see Fig. 3. In the inset in Fig. 3(a) one can see that, as $\Delta \rightarrow 1$, the differences between the predictions of the quench action approach and the GGE become of the order of 10%. Fig. 3(b) provides a closer look of $\langle \sigma_1^z \sigma_3^z \rangle$ in that regime. There, we also report our NLCE results [58]. The latter are consistent with the quench action predictions and inconsistent with the GGE results. Hence, our NLCE calculations support the correctness of the QA approach for describing observables after relaxation and the inability of the GGE constructed here to do so.

Conclusions. We used the quench action method to obtain an exact description of the steady state following a quench from the ground state of the Ising model to a XXZ spin-1/2 chain with anisotropy $\Delta \geq 1$. We were also able to fully implement a GGE based on all known local conserved charges. Our main finding is that the quench action steady state is different from the GGE prediction. We have shown that even for local correlators, the methods produce different results. An independent NLCE calculation supports the predictions of the quench action

approach. A possible interpretation of our results is that GGE based on the local charges Q_m is incomplete, and that a larger set of conserved (quasi- or nonlocal) charges is needed [70–72]. This makes apparent that the study of quantum quenches provides a unique venue to further deepen our understanding of the dynamics of interacting integrable models.

It also remains an interesting open problem to extend our results to the gapless regime $-1 < \Delta < 1$ and, going beyond steady-state issues, to reconstruct the post-quench time-dependent relaxation itself, which is accessible via a quench action treatment and which would make correspondence to eventual experimental realizations more direct. We will return to these and further applications of the quench action method in future work.

Acknowledgments. We would like to thank P. Calabrese, F. Essler, M. Fagotti, V. Gritsev, A. Klümper, R. Konik, M. Kormos, B. Pozsgay, and R. Vlijm for useful discussions. We acknowledge support from the Foundation for Fundamental Research on Matter (FOM), the Netherlands Organisation for Scientific Research (NWO), and the US Office of Naval Research. For their support and hospitality, MB, MR and J-SC thank the Perimeter Institute, and BW, JDN and J-SC thank CUNY (where the main results of this work were first made public). This work forms part of the activities of the Delta Institute for Theoretical Physics (D-ITP).

Note added. After our preprint appeared on the arXiv, another preprint [73] appeared which reports independent evidence that the quench action approach (and not the GGE on known local conserved charges) correctly predicts the steady state for the Néel-to-XXZ quench. Two other related preprints [74, 75] subsequently appeared on the arXiv.

-
- [1] T. Kibble, Phys. Rep. **67**, 183 (1980).
 [2] W. Zurek, Nature **317**, 505 (1985).
 [3] G. D. Moore and D. Teaney, Phys. Rev. C **71**, 064904 (2005).
 [4] M. C. Cross and P. C. Hohenberg, Rev. Mod. Phys. **65**, 851 (1993).
 [5] T. Chou, K. Mallick, and R. K. P. Zia, Rep. Prog. Phys. **74**, 116601 (2011).
 [6] J. Kurchan, Nature **433**, 222 (2005).
 [7] A. Polkovnikov, K. Sengupta, A. Silva, and M. Vengalattore, Rev. Mod. Phys. **83**, 863 (2011).
 [8] P. Calabrese and J. Cardy, Phys. Rev. Lett. **96**, 136801 (2006).
 [9] M. Rigol, V. Dunjko, V. Yurovsky, and M. Olshanii, Phys. Rev. Lett. **98**, 050405 (2007).
 [10] M. Rigol, A. Muramatsu, and M. Olshanii, Phys. Rev. A **74**, 053616 (2006).
 [11] M. Rigol, V. Dunjko, and M. Olshanii, Nature **452**, 854 (2008).
 [12] T. Barthel and U. Schollwöck, Phys. Rev. Lett. **100**, 100601 (2008).
 [13] M. Cramer and J. Eisert, New J. Phys. **12**, 055020 (2010).
 [14] A. C. Cassidy, C. W. Clark, and M. Rigol, Phys. Rev. Lett. **106**, 140405 (2011).
 [15] P. Calabrese, F. H. L. Essler, and M. Fagotti, Phys. Rev. Lett. **106**, 227203 (2011).
 [16] P. Calabrese, F. H. L. Essler, and M. Fagotti, J. Stat. Mech.: Th. Exp. , P07016 (2012).
 [17] P. Calabrese, F. H. L. Essler, and M. Fagotti, J. Stat. Mech.: Th. Exp. , P07022 (2012).
 [18] B. Pozsgay, J. Stat. Mech.: Th. Exp. , P07003 (2013).
 [19] M. Fagotti, M. Collura, F. H. L. Essler, and P. Calabrese, Phys. Rev. B **89**, 125101 (2014).
 [20] L. Bucciattini, M. Kormos, and P. Calabrese, J. Phys. A: Math. Theor. **47**, 175002 (2014).
 [21] P. Barmettler, M. Punk, V. Gritsev, E. Demler, and E. Altman, Phys. Rev. Lett. **102**, 130603 (2009).
 [22] P. Barmettler, M. Punk, V. Gritsev, E. Demler, and E. Altman, New J. Phys. **12**, 055017 (2010).
 [23] D. Rossini, A. Silva, G. Mussardo, and G. E. Santoro, Phys. Rev. Lett. **102**, 127204 (2009).
 [24] D. Rossini, S. Suzuki, G. Mussardo, G. E. Santoro, and A. Silva, Phys. Rev. B **82**, 144302 (2010).
 [25] A. Faribault, P. Calabrese, and J.-S. Caux, J. Math. Phys. **50**, 095212 (2009).
 [26] J. Mossel and J.-S. Caux, New J. Phys. **12**, 055028 (2010).
 [27] F. Iglói and H. Rieger, Phys. Rev. Lett. **106**, 035701 (2011).
 [28] M. C. Bañuls, J. I. Cirac, and M. B. Hastings, Phys. Rev. Lett. **106**, 050405 (2011).
 [29] W. Liu and N. Andrei, arXiv:1311.1118.
 [30] M. Rigol and M. Fitzpatrick, Phys. Rev. A **84**, 033640 (2011).
 [31] G. P. Brandino, A. De Luca, R. M. Konik, and G. Mussardo, Phys. Rev. B **85**, 214435 (2012).
 [32] E. Demler and A. M. Tsvelik, Phys. Rev. B **86**, 115448 (2012).
 [33] K. He and M. Rigol, Phys. Rev. A **85**, 063609 (2012).
 [34] K. He and M. Rigol, Phys. Rev. A **87**, 043615 (2013).
 [35] M. Heyl, A. Polkovnikov, and S. Kehrein, Phys. Rev. Lett. **110**, 135704 (2013).
 [36] B. Pozsgay, J. Stat. Mech.: Th. Exp. , P10028 (2013).
 [37] M. Fagotti, arXiv:1308.0277.
 [38] M. Heyl, arXiv:1403.4570.
 [39] M. Marcuzzi, J. Marino, A. Gambassi, and A. Silva, Phys. Rev. Lett. **111**, 197203 (2013).
 [40] G. Mussardo, Phys. Rev. Lett. **111**, 100401 (2013).
 [41] M. Kormos, A. Shashi, Y.-Z. Chou, J.-S. Caux, and A. Imambekov, Phys. Rev. B **88**, 205131 (2013).
 [42] F. H. L. Essler, S. Kehrein, S. R. Manmana, and N. J. Robinson, Phys. Rev. B **89**, 165104 (2014).
 [43] T. Kinoshita, T. Wenger, and D. S. Weiss, Nature **440**, 900 (2006).
 [44] S. Trotzky, Y.-A. Chen, A. Flesch, I. P. McCulloch, U. Schollwöck, J. Eisert, and I. Bloch, Nat. Phys. **8**, 325 (2012).
 [45] M. Cheneau, P. Barmettler, D. Poletti, M. Endres, P. Schauss, T. Fukuhara, C. Gross, I. Bloch, C. Kollath, and S. Kuhr, Nature **481**, 484 (2012).
 [46] M. Gring, M. Kuhnert, T. Langen, T. Kitagawa, B. Rauer, M. Schreitl, I. Mazets, D. A. Smith, E. Demler, and J. Schmiedmayer, Science **337**, 1318 (2012).
 [47] T. Fukuhara, P. Schauss, M. Endres, S. Hild, M. Cheneau, I. Bloch, and C. Gross, Nature **502**, 76 (2013).

- [48] J.-S. Caux and F. H. L. Essler, Phys. Rev. Lett. **110**, 257203 (2013).
- [49] M. Rigol, Phys. Rev. Lett. **112**, 170601 (2014).
- [50] M. Rigol, *in preparation*.
- [51] J. De Nardis, B. Wouters, M. Brockmann, and J.-S. Caux, Phys. Rev. A **89**, 033601 (2014).
- [52] B. Wouters, M. Brockmann, J. De Nardis, D. Fioretto, R. Vlijm, and J.-S. Caux, *in preparation*.
- [53] R. Orbach, Phys. Rev. **112**, 309 (1958).
- [54] H. Bethe, Zeit. für Physik **71**, 205 (1931).
- [55] M. Takahashi, Prog. Theor. Phys. **46**, 401 (1971).
- [56] V. E. Korepin, N. M. Bogoliubov, and A. G. Izergin, *Quantum Inverse Scattering Method and Correlation Functions* (Cambridge University Press, Cambridge, 1993).
- [57] M. Takahashi, *Thermodynamics of one-dimensional solvable models* (Cambridge University Press, Cambridge, 1999).
- [58] See supplementary material.
- [59] M. Brockmann, J. De Nardis, B. Wouters, and J.-S. Caux, J. Phys. A: Math. Theor. **47**, 145003 (2014).
- [60] M. Brockmann, J. De Nardis, B. Wouters, and J.-S. Caux, arXiv:1403.7469.
- [61] K. K. Kozłowski and B. Pozsgay, J. Stat. Mech.: Th. Exp. **2012**, P05021 (2012).
- [62] M. Rigol, T. Bryant, and R. R. P. Singh, Phys. Rev. Lett. **97**, 187202 (2006).
- [63] M. Rigol, T. Bryant, and R. R. P. Singh, Phys. Rev. E **75**, 061118 (2007).
- [64] M. P. Grabowski and P. Mathieu, Mod. Phys. Lett. A **9**, 2197 (1994).
- [65] M. P. Grabowski and P. Mathieu, Ann. Phys. **243**, 299 (1995).
- [66] J. Mossel and J.-S. Caux, J. Phys. A: Math. Theor. **45**, 255001 (2012).
- [67] J.-S. Caux and R. M. Konik, Phys. Rev. Lett. **109**, 175301 (2012).
- [68] M. Fagotti and F. H. L. Essler, J. Stat. Mech.: Th. Exp. , P07012 (2013).
- [69] M. Mestyán and B. Pozsgay, arXiv:1405.0232.
- [70] T. Prosen, Phys. Rev. Lett. **106**, 217206 (2011).
- [71] T. Prosen, arXiv:1406.2258.
- [72] R. G. Pereira, V. Pasquier, J. Sirker, and I. Affleck, arXiv:1406.2306.
- [73] B. Pozsgay, M. Mestyán, M. A. Werner, M. Kormos, G. Zaránd, and G. Takács, arXiv:1405.2843.
- [74] G. Goldstein and N. Andrei, arXiv:1405.4224.
- [75] B. Pozsgay, arXiv:1406.4613.

Supplementary Material for EPAPS

Quenching the Anisotropic Heisenberg Chain: Exact Solution and Generalized Gibbs Ensemble

THERMODYNAMIC LIMIT OF THE OVERLAPS

In order to apply the quench action logic we need to compute the thermodynamic limit of the overlap coefficients and in particular their leading extensive part

$$S[\rho] = \lim_{\text{th}} S_{\lambda} = -\lim_{\text{th}} \ln \frac{\langle \Psi_0 | \{\pm \lambda_j\}_{j=1}^{M/2} \rangle}{\|\{\pm \lambda_j\}_{j=1}^{M/2}\|}. \quad (\text{S1})$$

The procedure is to consider the overlap coefficient for a generic finite size Bethe state $|\{\lambda_j\}_{j=1}^M\rangle$ that in the thermodynamic limit, $N \rightarrow \infty$ with $M/N = 1/2$ fixed, flows to a set of distributions $|\{\lambda_j\}_{j=1}^M\rangle \rightarrow |\rho\rangle$. Equivalently, in the thermodynamic limit the eigenvalue of a smooth diagonal observable \mathcal{A} can be recast into a sum of integrals weighted by the distributions $\rho = \{\rho_n\}_{n=1}^{\infty}$:

$$\mathcal{A}|\{\lambda_j\}_{j=1}^M\rangle = \left[\sum_{j=1}^M A_j \right] |\{\lambda_j\}_{j=1}^M\rangle \rightarrow \left[N \sum_{n=1}^{\infty} \int_{-\pi/2}^{\pi/2} d\lambda \rho_n(\lambda) \tilde{A}_n(\lambda) \right] |\rho\rangle. \quad (\text{S2})$$

By assumption the extensive part of the overlap coefficient $S[\rho]$ is smooth and does not depend on finite size differences within the set of Bethe states that scale to the same densities ρ . The number of Bethe states for each set of distributions ρ is given by the extensive Yang-Yang entropy [1]: $e^{S_{\text{YY}}[\rho]}$. We are then free to select a representative finite size Bethe state out of all states that scale to the same ρ . We consider the state $|\{\lambda_j\}_{j=1}^M\rangle$ consisting of $2n_s$ strings such that $2n_s = \sum_{n=1}^{\infty} M_n$, where M_n is the number of n -strings in the state and we choose all M_n to be even. Note that this is one possible choice for a representative state. Different choices regarding the evenness of the fillings $\{M_n\}_{n=1}^{\infty}$ lead to different expressions for the exact overlap formula (S4), but are believed [2, 3] to have the same extensive smooth part $S[\rho]$.

For any finite size N , Bethe states are organized in deviated strings. We use the following notation to label the rapidities of such states:

$$\lambda_j \rightarrow \lambda_{\alpha}^{n,a} = \lambda_{\alpha}^n + \frac{i\eta}{2}(n+1-2a) + i\delta_{\alpha}^{n,a}, \quad (\text{S3})$$

where $a = 1, \dots, n$ and $\alpha = 1, \dots, M_n$. The string deviations $\delta_{\alpha}^{n,a}$ are vanishing in the thermodynamic limit. Though the string hypothesis is not systematically verified around the ground state of the zero-magnetized spin chain [4, 5], it is effectively verified away from the ground state, for example at finite temperatures [6], and by extension in the circumstances discussed here.

The finite size overlap formula between this class of representative states and the Néel state is given in Ref. [7],

$$\frac{\langle \Psi_0 | \{\pm \lambda_j\}_{j=1}^{M/2} \rangle}{\|\{\pm \lambda_j\}_{j=1}^{M/2}\|} = \gamma \times \sqrt{\frac{\det_{M/2}(G_{jk}^+)}{\det_{M/2}(G_{jk}^-)}} \quad \text{with} \quad \gamma = \prod_{j=1}^{M/2} \frac{\sqrt{\tan(\lambda_j + i\eta/2) \tan(\lambda_j - i\eta/2)}}{2 \sin(2\lambda_j)}. \quad (\text{S4})$$

The prefactor γ has to leading order no explicit system size dependence from the string deviations $\delta \rightarrow 0$, but is exponentially vanishing when the particle number M is sent to infinity due to the product over all rapidities. We focus on the ratio of the two determinants, where the matrices are given by

$$G_{(n,\alpha,a),(m,\beta,b)}^{\pm} = \delta_{(n,\alpha,a),(m,\beta,b)} \left(NK_{\eta/2}(\lambda_{\alpha}^{n,a}) - \sum_{(\ell,\gamma,c)} K_{\eta}^+(\lambda_{\alpha}^{n,a}, \lambda_{\gamma}^{\ell,c}) \right) + K_{\eta}^{\pm}(\lambda_{\alpha}^{n,a}, \lambda_{\beta}^{m,b}). \quad (\text{S5})$$

Here, $K_{\eta}^{\pm}(\lambda, \mu) = K_{\eta}(\lambda - \mu) \pm K_{\eta}(\lambda + \mu)$ and $K_{\eta}(\lambda) = \frac{\sinh(2\eta)}{\sin(\lambda + i\eta) \sin(\lambda - i\eta)}$. Divergences in system size as $1/\delta$ occur in each string block ($n = m, \alpha = \beta$) when $b = a + 1$ in the term $K_{\eta}(\lambda_{\alpha}^{n,a} - \lambda_{\alpha}^{n,a+1}) \sim \frac{i}{(\delta_{\alpha}^{n,a+1} - \delta_{\alpha}^{n,a})}$. On the other hand, for our representative state the terms $\pm K_{\eta}(\lambda + \mu)$ in G^{\pm} are never divergent since all string centers are strictly positive.

We conclude that the divergences in $1/\delta$ in $\det_{M/2}(G^+)$ cancel exactly the divergences in $\det_{M/2}(G^-)$, as they occur in exactly the same form. The same cancellation applies to divergences appearing in $K_\eta(\lambda - \mu)$ when two rapidities from different strings get close in the thermodynamic limit $\mu \rightarrow \lambda \pm i\eta + g(N)$ with $\lim_{\text{th}} g(N) = 0$. We are then able to take the thermodynamic limit \lim_{th} for the overlap coefficients analogously to Ref. [8]. Being non-exponential in system size, the ratio of the two determinants can then be neglected in the contribution to the overlaps that is leading in system size. The thermodynamic overlap coefficients then read as

$$S[\rho] = \lim_{\text{th}} S_\lambda = -\frac{N}{2} \sum_{n=1}^{\infty} \int_0^{\pi/2} d\lambda \rho_n(\lambda) \ln W_n(\lambda), \quad (\text{S6})$$

where

$$W_n(\lambda) = \frac{1}{2^{n+1} \sin^2 2\lambda} \frac{\cosh n\eta - \cos 2\lambda}{\cosh n\eta + \cos 2\lambda} \prod_{j=1}^{\frac{n-1}{2}} \left(\frac{\cosh(2j-1)\eta - \cos 2\lambda}{(\cosh(2j-1)\eta + \cos 2\lambda)(\cosh 4j\eta - \cos 4\lambda)} \right)^2, \quad (\text{S7})$$

if n odd, and

$$W_n(\lambda) = \frac{\tan^2 \lambda \cosh n\eta - \cos 2\lambda}{2^n \cosh n\eta + \cos 2\lambda} \frac{1}{\prod_{j=1}^{\frac{n}{2}} (\cosh 2(2j-1)\eta - \cos 4\lambda)^2} \prod_{j=1}^{\frac{n-2}{2}} \left(\frac{\cosh 2j\eta - \cos 2\lambda}{\cosh 2j\eta + \cos 2\lambda} \right)^2, \quad (\text{S8})$$

if n even.

GTBA EQUATIONS FOR THE NÉEL-TO-XXZ QUENCH

In this section we focus on the derivation of the saddle point state, specified by the set of distribution ρ^{sp} obtained by varying the quench action $S_{QA}[\rho] = 2S[\rho] - \frac{1}{2}S_{YY}[\rho]$ with respect to each root density $\rho_n(\lambda)$. Variation of the Yang-Yang entropy is well-known [1]. It should be noted that in front of the Yang-Yang entropy there is an extra factor $\frac{1}{2}$. The reason is that only parity-invariant Bethe states contribute and therefore the number of microstates in the ensemble ρ is the square root of the usual number of microstates. Furthermore, only states in the magnetization sector $M = N/2$ have non-zero overlap with the initial Néel state. In order to vary with respect to all $\rho_n(\lambda)$ independently, we need to add a Lagrange multiplier term to the quench action:

$$-hN \left(\sum_{m=1}^{\infty} m \int_{-\pi/2}^{\pi/2} d\lambda \rho_m(\lambda) - \frac{1}{2} \right), \quad (\text{S9})$$

where h is the Lagrange multiplier. Variation with respect to $\rho_n(\lambda)$ then leads to the saddle point conditions

$$\ln \eta_n(\lambda) = -2hn - \ln W_n(\lambda) + \sum_{m=1}^{\infty} a_{nm} * \ln(1 + \eta_m^{-1})(\lambda), \quad (\text{S10})$$

where $n \geq 1$, $\eta_n(\lambda) = \rho_{n,h}(\lambda)/\rho_n(\lambda)$ and the convolution $*$ is defined by

$$(f * g)(\lambda) = \int_{-\pi/2}^{\pi/2} d\mu f(\lambda - \mu)g(\mu) \quad (\text{S11})$$

The kernels are defined by $a_{nm}(\lambda) = (1 - \delta_{nm})a_{|n-m|}(\lambda) + 2a_{|n-m|+2}(\lambda) + \dots + 2a_{n+m-2}(\lambda) + a_{n+m}(\lambda)$, where

$$a_n(\lambda) = \frac{1}{\pi} \frac{\sinh(n\eta)}{\cosh(n\eta) - \cos(2\lambda)}. \quad (\text{S12})$$

The functions $-2hn - \ln(W_n)$ are called driving terms. For each fixed value of h the set (S10) of Generalized Thermodynamic Bethe Ansatz (GTBA) equations has a solution in terms of the functions η_n . Substituting this solution into thermodynamic Bethe equations leads to the saddle point distributions ρ^{sp} . The parameter h is fixed by the magnetization condition $M/N = 1/2$ of the initial Néel state,

$$\sum_{m=1}^{\infty} m \int_{-\pi/2}^{\pi/2} d\lambda \rho_m^{\text{sp}}(\lambda) = \frac{1}{2}. \quad (\text{S13})$$

As for the TBA equations at finite temperature [9], one can recast the GTBA Eqs. (S10) into a factorized form where there is no infinite sum over string lengths. We will now derive this result. We use the Fourier transform conventions

$$\hat{f}_k = \text{FT}[f](k) = \int_{-\pi/2}^{\pi/2} e^{2ik\lambda} f(\lambda) d\lambda, \quad k \in \mathbb{Z}, \quad (\text{S14})$$

$$f(\lambda) = \text{FT}^{-1}[\hat{f}](\lambda) = \frac{1}{\pi} \sum_{k \in \mathbb{Z}} e^{-2ik\lambda} \hat{f}_k. \quad (\text{S15})$$

The Fourier transforms of the kernels are $\hat{a}_{n,k} = e^{-|k|n\eta}$, and using the convolution theorem this implies $a_m * a_n = a_{m+n}$. A set of identities for the kernels can then be derived [9]

$$(a_0 + a_2) * a_{nm} = a_1 * (a_{n-1,m} + a_{n+1,m}) + (\delta_{n-1,m} + \delta_{n+1,m}) a_1, \quad n \geq 2, m \geq 1, \quad (\text{S16a})$$

and

$$(a_0 + a_2) * a_{1,m} = a_1 * a_{2,m} + a_1 \delta_{2,m}, \quad m \geq 1, \quad (\text{S16b})$$

where we used the convention $a_0(\lambda) = \delta(\lambda)$. Convolving the GTBA Eqs. (S10) with $(a_0 + a_2)$, the infinite sum can be removed, and we find that

$$(a_0 + a_2) * \ln(\eta_n) = (a_0 + a_2) * g_n - a_1 * (g_{n-1} + g_{n+1}) + a_1 * [\ln(1 + \eta_{n-1}) + \ln(1 + \eta_{n+1})]. \quad (\text{S17})$$

Here, the driving terms of the original GTBA equations are rewritten in a more convenient form with $g_n(\lambda) = -\ln W_n(\lambda) - 2n \ln 4$, where

$$g_n = \sum_{l=0}^{n-1} \ln \left[\frac{s_{n-1-2l} c_{n-1-2l} s_{-n+1+2l} c_{-n+1+2l}}{t_{n-2l} t_{-n+2l}} \right], \quad (\text{S18a})$$

$$t_n = \frac{s_n}{c_n}, \quad s_n(\lambda) = \sin \left(\lambda + \frac{i\eta n}{2} \right), \quad c_n(\lambda) = \cos \left(\lambda + \frac{i\eta n}{2} \right). \quad (\text{S18b})$$

Defining $g_0(\lambda) = 0$ and $\eta_0(\lambda) = 0$, Eq. (S17) holds for $n \geq 1$. Let us rewrite the new driving terms $\tilde{d}_n = (a_0 + a_2) * g_n - a_1 * (g_{n-1} + g_{n+1})$ of Eq. (S17). We first rewrite g_n such that only positive indices are present:

$$g_n = 2\delta_{n \bmod 2, 1} \ln \left[s_0^{(2)} \right] + 4 \sum_{l=1}^{\lfloor n/2 \rfloor} \ln \left[s_{n+1-2l}^{(2)} \right] + 2 \sum_{l=1}^{n-1} \ln \left[\frac{c_l^{(2)}}{s_l^{(2)}} \right] + \ln \left[\frac{c_0^{(2)}}{s_0^{(2)}} \right] + \ln \left[\frac{c_n^{(2)}}{s_n^{(2)}} \right], \quad (\text{S19})$$

where $s_l^{(2)} = s_l s_{-l}$, $c_l^{(2)} = c_l c_{-l}$ or, explicitly,

$$s_l^{(2)}(\lambda) = \sin \left(\lambda + \frac{i\eta l}{2} \right) \sin \left(\lambda - \frac{i\eta l}{2} \right) = \sin^2(\lambda) + \sinh^2 \left(\frac{\eta l}{2} \right), \quad (\text{S20a})$$

$$c_l^{(2)}(\lambda) = \cos \left(\lambda + \frac{i\eta l}{2} \right) \cos \left(\lambda - \frac{i\eta l}{2} \right) = \cos^2(\lambda) + \sinh^2 \left(\frac{\eta l}{2} \right). \quad (\text{S20b})$$

Now we use that for $\tilde{a}_\alpha(\lambda) = \frac{1}{2\pi} \frac{\sinh(2\alpha)}{\sin^2(\lambda) + \sinh^2(\alpha)}$ and $f_\beta(\lambda) = \ln[\sin^2(\lambda) + \sinh^2(\beta)]$ the following relation holds ($\alpha, \beta > 0$):

$$\tilde{a}_\alpha * f_\beta = f_{\alpha+\beta} - 2\alpha. \quad (\text{S21})$$

This implies the identities

$$a_m * \ln \left[\frac{c_l^{(2)}}{s_l^{(2)}} \right] = \ln \left[\frac{c_{l+m}^{(2)}}{s_{l+m}^{(2)}} \right], \quad a_l * \ln \left[\frac{s_0^{(2)}}{s_2^{(2)}} \right] = \ln \left[\frac{s_l^{(2)}}{s_{l+2}^{(2)}} \right] \quad \text{and} \quad a_l * \ln \left[\frac{c_0^{(2)}}{c_2^{(2)}} \right] = \ln \left[\frac{c_l^{(2)}}{c_{l+2}^{(2)}} \right]. \quad (\text{S22})$$

From this we can calculate \tilde{d}_{2n} and \tilde{d}_{2n-1} for all $n \geq 1$ explicitly:

$$\tilde{d}_{2n} = \ln \left[\frac{c_0^{(2)}}{c_2^{(2)}} \right] - \ln \left[\frac{s_0^{(2)}}{s_2^{(2)}} \right], \quad \tilde{d}_{2n-1} = \ln \left[\frac{c_0^{(2)}}{c_2^{(2)}} \right] + \ln \left[\frac{s_0^{(2)}}{s_2^{(2)}} \right]. \quad (\text{S23})$$

The GTBA equations can be written compactly as

$$(a_0 + a_2) * \ln(\eta_n) = \tilde{d}_n + a_1 * [\ln(1 + \eta_{n-1}) + \ln(1 + \eta_{n+1})], \quad (\text{S24a})$$

where $n \geq 1$, the λ -dependence is left implicit and by convention $\eta_0(\lambda) = 0$ and $a_0(\lambda) = \delta(\lambda)$. The driving terms are given by

$$\tilde{d}_n(\lambda) = \ln \left[\frac{\cos^2(\lambda)}{\cos^2(\lambda) + \sinh^2(\eta)} \right] - (-1)^n \ln \left[\frac{\sin^2(\lambda)}{\sin^2(\lambda) + \sinh^2(\eta)} \right]. \quad (\text{S24b})$$

Using the convolution theorem once again, one can invert the operation of $(a_0 + a_2)*$ and bring it to the right hand side of Eq. (S24a). The Fourier transforms of the driving terms are

$$\hat{\tilde{d}}_{n,k} = 2\pi \frac{(1 - e^{-2\eta|k|})}{|k|} \left(\frac{(-1)^n - (-1)^k}{2} \right). \quad (\text{S25})$$

Defining

$$\begin{aligned} \hat{d}_{n,k} &:= \frac{\hat{\tilde{d}}_{n,k}}{\hat{a}_{0,k} + \hat{a}_{2,k}} = 2\pi \frac{\tanh(\eta k)}{k} \left(\frac{(-1)^n - (-1)^k}{2} \right), \\ \hat{s}_k &:= \frac{\hat{a}_{1,k}}{\hat{a}_{0,k} + \hat{a}_{2,k}} = \frac{1}{2 \cosh(k\eta)}, \end{aligned} \quad (\text{S26})$$

the GTBA equations in Fourier space are

$$\text{FT}[\ln(\eta_n)](k) = \hat{d}_{n,k} + \hat{s}_k \left(\text{FT}[\ln(1 + \eta_{n-1})](k) + \text{FT}[\ln(1 + \eta_{n+1})](k) \right). \quad (\text{S27})$$

In real space they are precisely the GTBA equations of the main text.

NEAREST-NEIGHBOR SPIN-SPIN CORRELATION

In this section we show how to compute the expectation value of the nearest-neighbor spin-spin correlator, $\langle \sigma_j^z \sigma_{j+1}^z \rangle = 1 + \frac{4}{NJ} \langle \frac{\partial H}{\partial \Delta} \rangle$, in the thermodynamic limit on a generic, translationally invariant Bethe eigenstate specified by a set of smooth distributions $\boldsymbol{\rho}$. This is a direct consequence of the Hellmann-Feynman theorem [10]. Independently, an analogous implementation was recently presented in Ref. [11].

A naive application of the Hellmann-Feynman theorem on the saddle point state leads to a wrong result

$$\langle \boldsymbol{\rho}^{\text{sp}} | \frac{1}{N} \frac{\partial H}{\partial \Delta} | \boldsymbol{\rho}^{\text{sp}} \rangle \neq \frac{\partial}{\partial \Delta} \langle \boldsymbol{\rho}^{\text{sp}} | \frac{1}{N} H | \boldsymbol{\rho}^{\text{sp}} \rangle = -\frac{J}{2}. \quad (\text{S28})$$

This is because the overlaps of two Bethe states with different values of Δ are exponentially small in system size, which makes the thermodynamic limit and the derivative with respect to Δ noncommuting,

$$\lim_{\delta \rightarrow 0} \lim_{\text{th}} \langle \boldsymbol{\lambda}(\Delta) | \boldsymbol{\lambda}(\Delta + \delta) \rangle \neq \lim_{\text{th}} \lim_{\delta \rightarrow 0} \langle \boldsymbol{\lambda}(\Delta) | \boldsymbol{\lambda}(\Delta + \delta) \rangle. \quad (\text{S29})$$

In order to apply the Hellmann-Feynman theorem we need to take the derivative of the energy eigenvalue of a generic Bethe state at finite size N and then take the thermodynamic limit. Under the string hypothesis the energy eigenvalue $\omega_{\boldsymbol{\lambda}}$ becomes a function only of the string centers λ_{α}^n of the Bethe state, since the string deviations vanish exponentially in system size,

$$\omega_{\boldsymbol{\lambda}} = -\pi J \sinh(\eta) \sum_{n,\alpha} a_n(\lambda_{\alpha}^n), \quad (\text{S30})$$

where a_n is defined in Eq. (S12). We can now apply the Hellmann-Feynman theorem to this finite size state by taking the derivative of the energy with respect to Δ :

$$\langle \boldsymbol{\lambda} | \sigma_1^z \sigma_2^z | \boldsymbol{\lambda} \rangle = 1 + \frac{4}{NJ} \frac{d\omega_{\boldsymbol{\lambda}}}{d\Delta} = 1 + \frac{4}{NJ} \frac{1}{\sinh \eta} \frac{d\omega_{\boldsymbol{\lambda}}}{d\eta} = 1 - \frac{4\pi}{N} \sum_{n,\alpha} \left[\frac{\cosh \eta}{\sinh \eta} a_n(\lambda_{\alpha}^n) + (\partial_{\eta} a_n)(\lambda_{\alpha}^n) + \partial_{\lambda_{\alpha}^n} a_n(\lambda_{\alpha}^n) \frac{d\lambda_{\alpha}^n}{d\eta} \right]. \quad (\text{S31})$$

The quantities $\frac{d\lambda_\alpha^n}{d\eta}$ are obtained by deriving the reduced Bethe equations for string centers [12, 13]

$$\theta_n(\lambda_\alpha^n) - \frac{1}{N} \sum_{m,\beta} \theta_{nm}(\lambda_\alpha^n - \lambda_\beta^m) = \frac{2\pi}{N} I_\alpha^n \quad (\text{S32})$$

(see [9] for the definitions of θ_n and θ_{nm}) with respect to the interaction parameter η ,

$$N \tilde{a}_n(\lambda_\alpha^n) - \sum_{m,\beta} \tilde{a}_{nm}(\lambda_\alpha^n - \lambda_\beta^m) + \sum_{m,\beta} G_{(n,\alpha),(m,\beta)} \frac{d\lambda_\beta^m}{d\eta} = 0. \quad (\text{S33})$$

Here we introduced the reduced Gaudin matrix for string centers [14]

$$G_{(n,\alpha),(m,\beta)} = \delta_{(n,\alpha),(m,\beta)} \left(N a_n(\lambda_\alpha^n) - \sum_{k,\gamma} a_{nk}(\lambda_\alpha^n - \lambda_\gamma^k) \right) + a_{nm}(\lambda_\alpha^n - \lambda_\beta^m) \quad (\text{S34})$$

and the functions \tilde{a}_n and \tilde{a}_{nm} ,

$$\tilde{a}_n(\lambda) = \frac{1}{2\pi} \partial_\eta \theta_n(\lambda) = -a_n(\lambda) \frac{n \sin 2\lambda}{2 \sinh n\eta}, \quad (\text{S35})$$

$$\tilde{a}_{nm}(\lambda) = \frac{1}{2\pi} \partial_\eta \theta_{nm} = (1 - \delta_{nm}) \tilde{a}_{|n-m|}(\lambda) + 2\tilde{a}_{|n-m|+2}(\lambda) + \dots + 2\tilde{a}_{n+m-2}(\lambda) + \tilde{a}_{n+m}(\lambda). \quad (\text{S36})$$

We define a set of the auxiliary functions $\mathbf{h} = \{h_n\}_{n=1}^\infty$ such that

$$h_n(\lambda_\alpha^n) = \sum_{m,\beta} (G^{-1})_{(n,\alpha),(m,\beta)} \left(N \tilde{a}_m(\lambda_\beta^m) - \sum_{k,\gamma} \tilde{a}_{mk}(\lambda_\beta^m - \lambda_\gamma^k) \right). \quad (\text{S37})$$

In the thermodynamic limit, expression (S31) can then be recast as a functional of the distributions $\boldsymbol{\rho}$ and the auxiliary functions \mathbf{h} ,

$$\langle \boldsymbol{\rho} | \sigma_1^z \sigma_2^z | \boldsymbol{\rho} \rangle = 1 + \lim_{\text{th}} \frac{4}{NJ} \frac{d\omega_\lambda}{d\Delta} = 1 - 4\pi \sum_{n=1}^\infty \int_{-\pi/2}^{\pi/2} d\lambda \rho_n(\lambda) \left[\frac{\cosh \eta}{\sinh \eta} a_n(\lambda) + \partial_\eta a_n(\lambda) - (\partial_\lambda a_n(\lambda)) h_n(\lambda) \right], \quad (\text{S38})$$

where the auxiliary functions are determined by a set of linear integral equations

$$\rho_{n,t}(\lambda) h_n(\lambda) + \sum_{m=1}^\infty a_{nm} * (\rho_m h_m)(\lambda) = \tilde{a}_n(\lambda) - \sum_{m=1}^\infty \tilde{a}_{nm} * \rho_m(\lambda). \quad (\text{S39})$$

As in the case of GTBA Eqs. (S10), they can be reduced to

$$(a_0 + a_2) * (\rho_{n,t} h_n) = \left[(a_0 + a_2) * d_n - a_1 * (d_{n-1} + d_{n+1}) \right] + a_1 * (h_{n-1} \rho_{n-1,h} + h_{n+1} \rho_{n+1,h}), \quad (\text{S40})$$

with $h_0(\lambda) = d_0(\lambda) = 0$ and the driving terms given by ($n \geq 1$)

$$d_n(\lambda) = \tilde{a}_n(\lambda) - \sum_{m=1}^\infty \tilde{a}_{nm} * \rho_m(\lambda). \quad (\text{S41})$$

Analogously to the local conserved charges, the correlator (S38) can be expressed solely in terms of $\rho_{1,h}$ and the auxiliary function h_1 (see [3]),

$$\begin{aligned} \langle \boldsymbol{\rho} | \sigma_1^z \sigma_2^z | \boldsymbol{\rho} \rangle = 1 + 4 \left\{ - \frac{\cosh \eta}{\sinh \eta} \sum_{k \in \mathbb{Z}} \left(\frac{e^{-|k|\eta} - \hat{\rho}_{1,h}(k)}{2 \cosh k\eta} \right) + \sum_{k \in \mathbb{Z}} |k| \left[\frac{e^{-|k|\eta}}{2 \cosh k\eta} + \tanh(|k|\eta) \left(\frac{e^{-|k|\eta} - \hat{\rho}_{1,h}(k)}{2 \cosh k\eta} \right) \right] \right. \\ \left. - \pi \int_{-\pi/2}^{\pi/2} d\lambda \rho_{1,h}(\lambda) h_1(\lambda) \frac{\partial}{\partial \lambda} s(\lambda) \right\}, \quad (\text{S42}) \end{aligned}$$

where the function s is given in the main text and $\hat{\rho}_{1,h}$ is the Fourier transform, defined in (S14), of $\rho_{1,h}$.

NUMERICAL LINKED-CLUSTER EXPANSIONS

In this section we discuss the numerical linked-cluster expansion (NLCE) results. Such an expansion allows us to obtain the infinite-time average, or the diagonal ensemble (DE), result for the expectation value of spin-spin correlations. This approach was introduced in Ref. [15] to study quenches with initial thermal states. It can be straightforwardly tailored to study quenches with initial ground states as explained in detail, for the particular quenches considered in this work, in Ref. [16]. Here we report the results that are relevant to the discussion in the main text.

The NLCE calculations are done in clusters with up to 18 sites, as in Ref. [15]. We denote as $\mathcal{O}_l^{\text{DE}}$ the result obtained for an observable \mathcal{O} when adding the contribution of all clusters with up to l sites. We should stress that while the convergence of the NLCE calculations improves for increasing values of Δ [16], for large Δ they do not allow us to discriminate between the results of the quench action (QA) and the GGE calculations, which are very close to each other. They also do not allow us to discriminate between the QA and GGE results as $\Delta \rightarrow 1$ when the observable considered is $\sigma_1^z \sigma_2^z$. In that regime, the QA and GGE results are also too close to each other, becoming identical for $\Delta = 1$. As shown in Fig. 3 of the main text, the largest relative differences between the QA and GGE predictions are seen for $\langle \sigma_1^z \sigma_3^z \rangle$ when $\Delta \rightarrow 1$. This is the observable and regime in which we focus our NLCE effort.

In Fig. 4, we show results for $\langle \sigma_1^z \sigma_3^z \rangle_l^{\text{DE}}$ versus l for several values of Δ between 1 and 3. A few remarks are in order on those results. They can be seen to be converging with increasing l , the amplitude of the oscillations decreases, but do not quite converge for the cluster sizes accessible to us. As Δ decreases from 3, one can see that the convergence of the NLCE initially worsens, the amplitude of the oscillations increases for any two contiguous values of l , and then improves very close to $\Delta = 1$. Finally, it is apparent that the results for $\langle \sigma_1^z \sigma_3^z \rangle^{\text{DE}}$ decrease with decreasing Δ , as expected from the exact calculations discussed in the main text.

We now turn our attention to the regime in which Δ is very close to 1. The fact that the convergence of our NLCE calculations improves in that regime is better seen in Fig. 5, where we report results for $\Delta = 1, 1.01, 1.1, \text{ and } 1.2$. However, the results of our bare NLCE sums still do not allow us to discriminate between the QA and GGE results for $\Delta = 1$, which are depicted as continuous and dashed horizontal lines, respectively. As discussed in NLCE studies of systems in thermal equilibrium [17, 18], whenever NLCE series do not converge to a desired accuracy, one can use resummation techniques to accelerate the convergence of the series and obtain more accurate results. There are two resummation techniques that were explained in detail in Ref. [18], which we have found to improve convergence in our problem. Those are Wynn's and Brezinski's algorithms. They can be applied multiple times (in what we call "cycles") to a series for an observable and are expected to improve convergence with each cycle. However, the application of too many cycles can also lead to numerical instabilities [18].

In a nutshell, every cycle of those algorithms leads to a new series with fewer elements [18]. The last element after each cycle is expected to approach the $l \rightarrow \infty$ result. The reduction in the number of elements after each cycle limits the number of times each algorithm can be applied to a series. In Wynn's algorithm, each cycle reduces the number

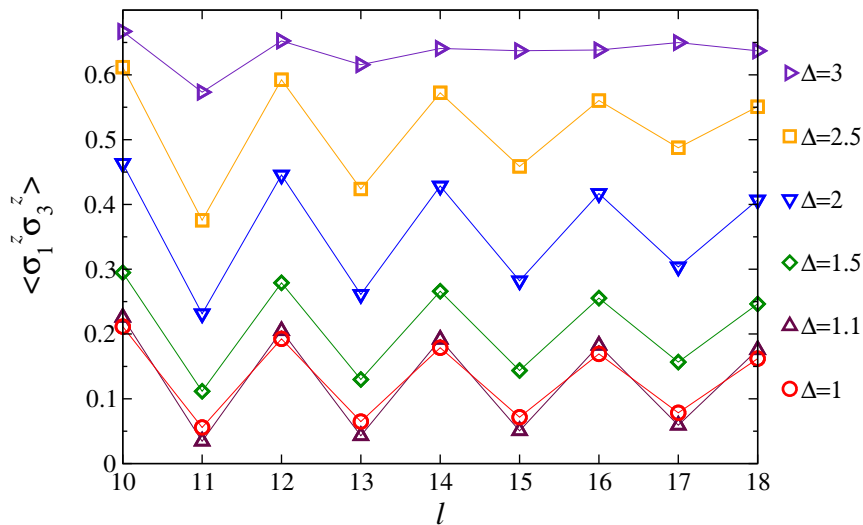


FIG. 4. Next-nearest neighbor correlations $\langle \sigma_1^z \sigma_3^z \rangle_l^{\text{DE}}$ versus l for quenches with $\Delta = 1, 1.1, 1.5, 2, 2.5, \text{ and } 3$. Results are reported for the last nine orders of the NLCE.

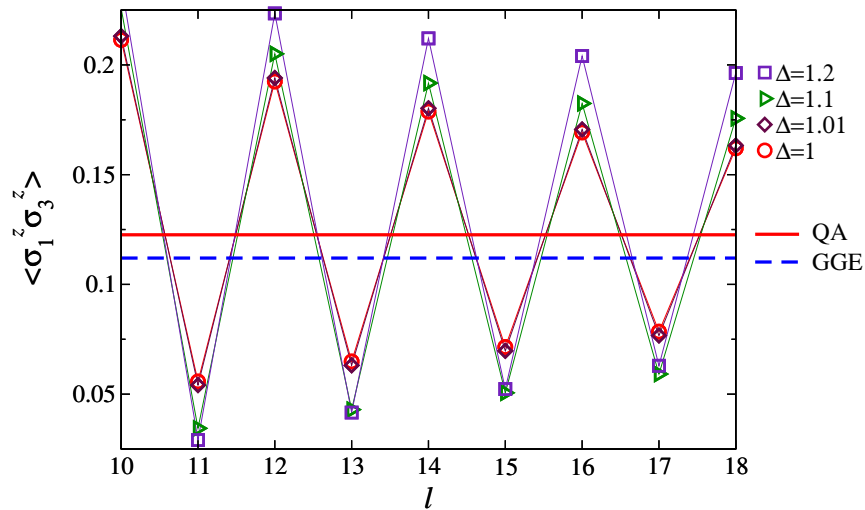


FIG. 5. Next-nearest neighbor correlations $\langle \sigma_1^z \sigma_3^z \rangle_l^{\text{DE}}$ versus l for quenches with $\Delta = 1, 1.01, 1.1,$ and 1.2 . Results are reported for the last nine orders of the NLCE. The QA and GGE predictions for $\Delta = 1$ are reported as continuous and dashed horizontal lines, respectively.

of elements by two, and in Brezinski's algorithm each cycle reduces the number of elements by three. Since our bare series for $\langle \sigma_1^z \sigma_3^z \rangle^{\text{DE}}$ has 18 elements (we consider clusters with up to 18 sites), the maximal number of cycles we can apply for Wynn's algorithm is 8 and for Brezinski's algorithm is 5.

In Fig. 6 we report the results (the last element) after each cycle of Wynn's and Brezinski's algorithms. As Δ approaches 1, we find that the resummations are stable and lead to very close results. This gives us confidence in the robustness of the resummations around the Heisenberg point. Figure 6 shows that, as $\Delta \rightarrow 1$ and as the number of cycles increases, Brezinski's algorithm appears to converge to a slightly larger value of $\langle \sigma_1^z \sigma_3^z \rangle^{\text{DE}}$ than the QA prediction, while Wynn's resummations seem to converge to a result slightly below the QA prediction. Both are far from the GGE prediction. Hence, our NLCE results support the correctness of the QA predictions for the outcome of the relaxation dynamics in these systems.

In the main text, we report the results of Brezinski's resummations after one cycle as representative of the outcome of the resummation techniques used. This because those results are almost identical to the ones obtained using Wynn's algorithm after one cycle, and are in between the results obtained after the maximal number of cycles that

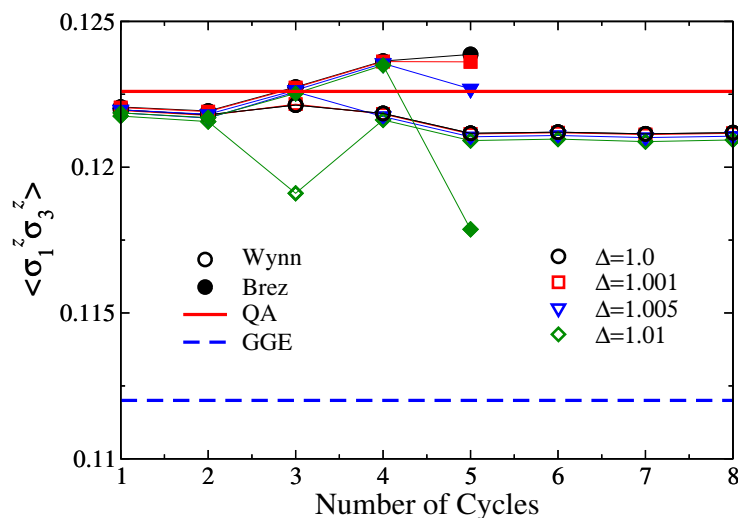


FIG. 6. Next-nearest neighbor correlations $\langle \sigma_1^z \sigma_3^z \rangle^{\text{DE}}$ after each cycle of Wynn's (empty symbols) and Brezinski's (filled symbols) algorithms. Results are reported for $\Delta = 1, 1.001, 1.005,$ and 1.01 , and are compared to the QA (continuous line) and GGE (dashed line) results for $\Delta = 1$.

could be applied in each algorithm. In the main text, we also report an interval of confidence that contains all results obtained within Brezinski's and Wynn's resummations, except for $\Delta = 0.015$ for which the last cycle of Brezinski's algorithm resulted in $\langle \sigma_1^z \sigma_3^z \rangle^{\text{DE}} = 0.1346$, which is out of the interval of confidence reported. We should add that the fluctuations in the values of Δ after resummations increase as Δ increases for $\Delta < 2$. Because of this, and the fact that the QA and GGE results approach each other with increasing Δ , we cannot use our NLCE results to discriminate between the QA and GGE predictions as one moves further away from the Heisenberg point.

-
- [1] V. E. Korepin, N. M. Bogoliubov, and A. G. Izergin, *Quantum Inverse Scattering Method and Correlation Functions* (Cambridge University Press, Cambridge, 1993).
 - [2] J.-S. Caux and F. H. L. Essler, *Phys. Rev. Lett.* **110**, 257203 (2013).
 - [3] B. Wouters, M. Brockmann, J. De Nardis, D. Fioretto, R. Vlijm, and J.-S. Caux, *in preparation*.
 - [4] F. Woynarovich, *J. Phys. A: Math. Gen.* **15**, 2985 (1982).
 - [5] O. Babelon, H. J. de Vega, and C. M. Viallet, *Nucl. Phys. B* **220**, 13 (1983).
 - [6] A. M. Tselik and P. B. Wiegmann, *Adv. Phys.* **32**, 453 (1983).
 - [7] M. Brockmann, J. De Nardis, B. Wouters, and J.-S. Caux, *J. Phys. A: Math. Theor.* **47**, 145003 (2014).
 - [8] J. De Nardis, B. Wouters, M. Brockmann, and J.-S. Caux, *Phys. Rev. A* **89**, 033601 (2014).
 - [9] M. Takahashi, *Thermodynamics of one-dimensional solvable models* (Cambridge University Press, Cambridge, 1999).
 - [10] R. P. Feynman, *Phys. Rev.* **56**, 340 (1939).
 - [11] M. Mestyan and B. Pozsgay, arXiv:1405.0232.
 - [12] H. Bethe, *Zeit. für Physik* **71**, 205 (1931).
 - [13] M. Takahashi, *Prog. Theor. Phys.* **46**, 401 (1971).
 - [14] J.-S. Caux, R. Hagemans, and J. M. Maillet, *J. Stat. Mech.: Th. Exp.* **2005**, P09003 (2005).
 - [15] M. Rigol, *Phys. Rev. Lett.* **112**, 170601 (2014).
 - [16] M. Rigol, *in preparation*.
 - [17] M. Rigol, T. Bryant, and R. R. P. Singh, *Phys. Rev. Lett.* **97**, 187202 (2006).
 - [18] M. Rigol, T. Bryant, and R. R. P. Singh, *Phys. Rev. E* **75**, 061118 (2007).